Theor Chem Acc (2015) 134:27
DOI 10.1007/s00214-015-1628-4

REGULAR ARTICLE

# The ligand effect on the selective C–H versus C–C bond activation of propane by $NiBr^+$: a theoretical study

**Lianming Zhao · Qiuyue Ding · Wenbin Xu · Pengpeng Sang · Xiaoli He · Zemin Shi · Yuhua Chi · Xiaoqing Lu · Wenyue Guo**

Received: 2 December 2014 / Accepted: 27 January 2015 / Published online: 12 February 2015


**Abstract** Density functional theory has been employed to investigate the ligand effect in the reaction of ligated $NiBr^+$ with propane. Both initial C–H and C–C bond activation mechanisms for losses of HBr, $H_2$, and $CH_4$ are analyzed in terms of the topology of the potential energy surface. Losses of HBr and $H_2$ involve three C–H activation mechanisms, that is, $\alpha,\beta$-H, $\alpha,\gamma$-H, and $\beta,\alpha$-H abstractions, where the last $\beta,\alpha$-H abstraction is the most favorable mechanism. Loss of $CH_4$ involves initial C–C activation, but it is prevented by the high-energy barrier. When propane reacts with the open-shell ligated $NiBr^+$, the ligand of Br in the initial C–H activation could direct abstract a H atom from propane substrate via a four-center transition state, without forming multi-$\sigma$-type bonding of $Ni^+$, whereas the metal center in the initial C–C activation needs to experience an unfavorable three $\sigma$-type bonding (with Br, $CH_3$, and $CH_2CH_3$), which explains why HBr and $H_2$ are formed in the reaction of $BrNi^+/C_3H_8$ and $CH_4$ not.

**Keywords** Density functional theory · Ligand effect · Potential energy surface

## 1 Introduction

Transition metal ions are of fundamental interesting in chemical and biology researches in the field of catalytic process. Because transition metal ions contain incompletely filled d or f orbits, they can supply electrons to ligands and accept electrons from ligands and thus have favorably catalytic activity. In order to deeply understand their intrinsic binding properties and reactivities, over the past three decades, a huge number of papers have been devoted to the investigation of the reactions of transition metal ions with organic molecules in the gas phase by using the experimental and theoretical methods [1–7]. In particular, the gas-phase reaction of bare transition metal ions with alkanes has undergone extensive investigation [8–31], which involves in the first three transition periods of metal. Interestingly, further study found that the introduction of ligands could change the reaction activity of metal ion greatly. Closed-shell ligand L (such as carbonyl, alkene, and phosphine) can through the electronic supply or feedback effect change electronic structure of the metal ion and may bring spatial constraints to the metal ions. Open-shell ligand X (such as halogen, hydroxyl, and cyclopentadienyl) can also change the electronic states of the metal ions via formation of the polarized covalent bonds, thereby leading to the change of thermal chemical property, ionization energy, binding energy, and even spin state of the metal ions. Generally, closed-shell ligand L only has an effect on the reaction efficiency of metal ions, whereas the influence of open-shell ligand X is according to the actual situation.

**Electronic supplementary material** The online version of this article (doi:10.1007/s00214-015-1628-4) contains supplementary material, which is available to authorized users.

L. Zhao (✉) · Q. Ding · W. Xu · P. Sang · X. He · Z. Shi · Y. Chi · X. Lu · W. Guo (✉)
College of Science, China University of Petroleum, Qingdao 266580, Shandong, People's Republic of China
e-mail: lmzhao@upc.edu.cn

W. Guo
e-mail: wyguo@upc.edu.cn

L. Zhao · Q. Ding · W. Xu · P. Sang · X. He · Z. Shi · Y. Chi · X. Lu · W. Guo
Key Laboratory of New Energy Physics and Materials Science in Universities of Shandong, China University of Petroleum, Qingdao 266580, Shandong, People's Republic of China

In all kinds of open-shell ligands, halogen X (X = F, Cl, Br, and I) is well known as the prototype of the class of covalent ligands [32–35]. Because of the large electronegativity and poor donor properties, halogen could form strongly polarized covalent bond to metals, and thus, it controls the reaction efficiency largely and even changes the product of the reaction. For example, bare $Cr^+$ is one of the least reactive transition metal ions, whereas $CrCl^+$ is significantly more reactive [36], and $CrF^+$ is even capable of dehydrogenating propane [37]. Under thermal conditions, both $PtCl^+$ and $PtCl_2^+$ could react with methane giving rise to HCl, while in the case of $PtBr^+$, formation of the corresponding carbine takes place. In order to understand the influence that ligand X (X = F, Cl, Br, and I) brings to the reactivity of $NiX^+$/RH (R = H, $C_2H_5$, $nC_3H_7$, and $nC_4H_9$) system, Schlangen et al. [38] have studied the gas-phase reaction of $NiX^+$/RH by using the electrospray ion (ESI) mass spectrum technology. They inferred that the reaction of $NiBr^+/C_3H_8$ exclusively involves initial C–H activation for losses of HBr and $H_2$, rather than initial C–C activation (for formation of $CH_4$). In this paper, we select the $NiBr^+ + C_3H_8$ reaction as a model of our theoretical study to discuss the C–H and C–C bond activation mechanisms (see Scheme 1). We hope to determine the essential factors that ligand controls the selectivity of the $NiBr^+/C_3H_8$ reaction.

### 1.1 Computational details

The geometry optimization and frequency calculations were carried out for all the relevant species using the B3LYP [39, 40] functional together with the DZVP(*d*)(opt + 3*f*) basis set [41] for $Ni^+$ and the 6-311++G(2*d*,2*p*) basis set [42] for nonmetal atoms. All the energies are reported with zero-point energy (ZPE) corrections with a scaling factor of 0.961 [43]. The DZVP(*d*)(opt) sets built up by Chiodo et al. have presented a good reliability for the B3LYP method in predicting transition metal ion ground- and excited-state order and splitting [41, 44]. The selected method has been proven to combine reasonable computational cost with accuracy sufficient for describing open-shell metal systems [43]. The intrinsic reaction coordinate (IRC) was performed to check the pathways between transition states and their connecting minima. Besides, the natural bond orbital (NBO) theory [45, 46] was used to shed new light on the characters of some important species involved. Dispersion energy was calculated to evaluate the dispersion contribution using ωB97X-D method with the DZVP(*d*)(opt + 3*f*): 6-311++G(2*d*,2*p*) basis set [47–49]. We confirmed the minimum energy crossing point (MECP) via single-point energy calculation of both considered states at the DZVP(*d*)(opt + 3*f*): 6-311++G(2*d*,2*p*) level for the relevant IRC points along the singlet pathway until they reach an equal energy. All these calculations were performed using the Gaussian 09 package [50].

The calculation methods of spin–orbit coupling (SOC) and crossing probability at the MECP, which has been described previously [51], are presented in detail in supporting information (SI). In brief, by using the GAMESS package [52], CASSCF calculations were first performed for both states at the MECP to get the converged CASSCF wave functions. The SOC value is the matrix element that expresses the coupling of the singlet and triplet states by the operator of Eq. 1 [53],

$$\langle \mathbf{H}_{\mathrm{SO}} \rangle_{S,S'} = \left\langle {}^1\Psi_1(\mathbf{M}_S) | \mathbf{H}_{\mathrm{SO}} | {}^3\Psi_2(\mathbf{M}_{S'}) \right\rangle. \tag{1}$$

Here, ${}^1\Psi_1$ (${}^3\Psi_2$) is the $\mathbf{M}_S$ ($\mathbf{M}_{S'}$) component of the many-body singlet-state (triplet-state) wave function. Considering the generated spin sublevels $\mathbf{M}_S$, a reasonable measure of the SOC-induced triplet–quintet interaction is the root-mean-square coupling constant (SOCC) of Eq. 2.

$$\mathrm{SOCC} = \left[ \sum_{S,S'} \langle \mathbf{H}_{\mathrm{SO}} \rangle^2_{S,S'} \right]^{1/2}. \tag{2}$$

A crude estimation of the crossing probability at the MECP can be done using the Landau–Zener formula [54–56],

$$P = 1 - e^{-2\delta},$$
$$\delta = \frac{\pi \left| V_{ij} \right|^2}{\hbar v \left| \Delta g_{ij} \right|} = \frac{\pi |\mathrm{SOCC}|^2}{(2\min(S_i, S_j) + 1)\hbar v \left| \Delta g_{ij} \right|}, \tag{3}$$

where $V_{ij}$ is a matrix element of a diabatic operator (SOC in this case) coupling two adiabatic states *i* and *j*, $\Delta g_{ij}$ is the difference in the gradients of the two adiabatic states *i* and *j*, and *v* is the effective velocity with which the system is passing through the crossing point that can be calculated from the kinetic theory of gases at 298 K.

## 2 Results and discussion

In the following sections, we will first establish the accuracy that is expected from the chosen level of theory for the $NiBr^+/C_3H_8$ system. Then, we will present structures and energies of reactants, products, and encounter complexes. Last, we will examine the title reaction in detail, including geometries of various stationary points and PESs. For simplicity, optimized geometries, selected structural parameters, calculated total energies, zero-point energies as well as $\langle S^2 \rangle$ values for all the species involved in the reaction are given in SI.

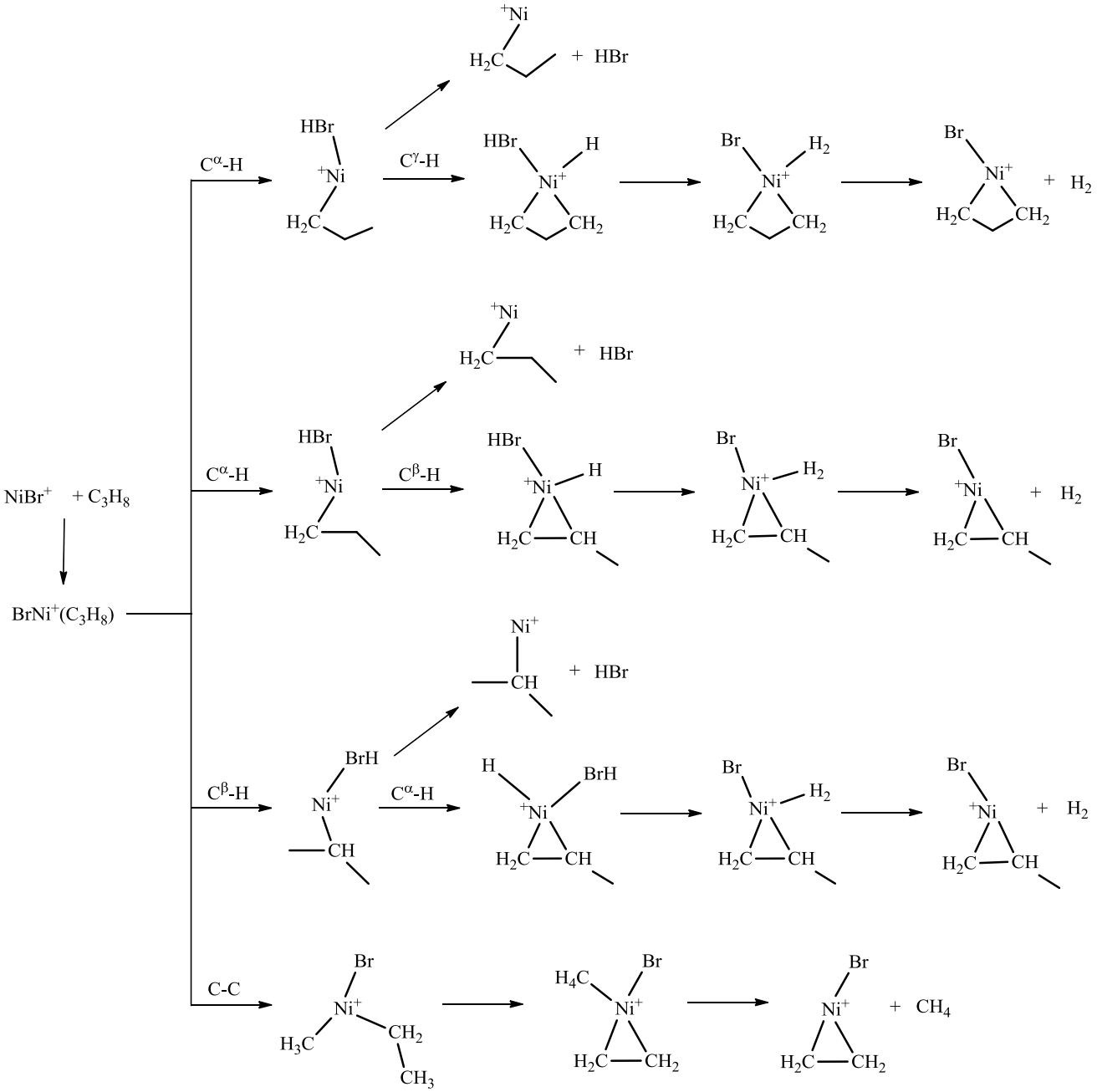


**Scheme 1** Schematic reaction mechanism of $C_3H_8$ with $NiBr^+$

## 2.1 Calibration

To evaluate the reliability of the level of theory employed, we compare the experimental thermochemical data with the results from the B3LYP approach. Table 1 collects the theoretically predicted adiabatic bond dissociation energies (BDEs) and the most reliable experimental data for some relevant species [57–69].

As shown in Table 1, the calculated excitation energy of $Ni^+$ ($^2D(d^9) \rightarrow {}^4F(d^8s^1)$) agrees well with the experimental gap value (20.1 vs 24.9 kcal/mol [57]). Moreover, the theoretical BDEs of H–Br and H–$C_3H_7$ accord well with the experimental findings. Our calculated bonding in $Ni^+$–X (X = H, $CH_2$, $CH_4$, $C_2H_4$, and $C_2H_6$) is overestimated by about 4–7 kcal/mol, which may be considered as a systematic shortcoming of the B3LYP functional. It should be noted that the calculated BDE of $Ni^+$–Br is underestimated by 13.4 kcal/mol based on the datum derived by Allison and Ridge [69]. Thus, the relative stability of the HBr + $[C_3, H_7, Ni]^+$ asymptote with respect to the

**Table 1** Adiabatic bond dissociation energies (kcal/mol) at 0 K determined by calculations and experiments

| Species | Calcd[a] | Expt |
|---|---|---|
| $Ni^+(^2D(d^9) \rightarrow {}^4F(d^8s^1))$ | 20.1 | 24.9[b] |
| H–Br | 88.3 | 87.5[c] |
| $CH_3CH_2CH_2$–H | 97.8 | 100.9 ± 0.5[c] |
| $Ni^+$–Br | 55.7 | >69.1[n] |
| $Ni^+$–H | 50 | 37.8 ± 1.8[j]; 42.9 ± 2.1[h]; 59.5 ± 3.7[g] |
| $Ni^+$–$CH_2$ | 79.2 | 73.1 ± 1[c]; 75.2 ± 1.6[m];86.4 ± 5.8[d] |
| $Ni^+$–$CH_4$ | 28.4 | 23.1 ± 1[c], 24.9[i] |
| $Ni^+$–$C_2H_4$ | 55.6 | 43.6 ± 2.5[k]; 44 ± 5[l]; 48.4 ± 9.2[f] |
| $Ni^+$–$C_2H_6$ | 35.6 | 28.7 ± 3.0[e] |

[a] At the B3LYP/DZVP(*d*)(opt + 3*f*): 6-311++G(2*d*,2*p*) level. [b] Ref. [57]. [c] Ref. [58]. [d] Ref. [59]. [e] Ref. [60]. [f] Ref. [61]. [g] Ref. [62]. [h] Ref. [63]. [i] Ref. [64]. [j] Ref. [65]. [k] Ref. [66]. [l] Ref. [67]. [m] Ref. [68]. [n] Ref. [69]

remainder of the $[C_3, H_8, Br, Ni]^+$ potential energy surface (PES) is probably underestimated by about 13 kcal/mol. However, the relative energies of the other parts of the PES are still described more satisfactorily. Such a situation has also been found for the PESs of the $Co^+/C_2H_6$, $Co^+/C_2H_6/N_2O$, $Fe^+/C_2H_6$, and $Fe^+/C_2H_6/N_2O$ systems calculated using density functional theory (DFT) [70–73].

To evaluate the dispersion contribution in the $NiBr^+/C_3H_8$ system, dispersion energies (DBs) were calculated using ωB97X-D method [47–49]. Calculated DB values for the species involved in the α,γ-H abstraction mechanism are given in Table S2. It is found that the DBs of $NiBr^+$, $H_2$, and HBr are zero nearly, while the values of $C_3H_8$ and other product ions ($[NiCH_2CH_2CH_3]^+$ (**$^1$Ia**) and $[NiBrCH_2CH_2CH_2]^+$ (**Ja**)) are 2.5 and 3.0–3.6 kcal/mol, respectively. For the intermediates and transition states involved, the DBs are calculated to be 3.8–4.6 kcal/mol. All these suggest that the dispersion contribution is relatively small and has a negligible effect on the relative energies of the $[C_3, H_8, Br, Ni]^+$ PES.

## 2.2 Reactants, encounter complexes, and products

In this section, we will discuss the structures and energies of reactants, encounter complexes, and products involved in the reaction of $NiBr^+/C_3H_8$. The optimized geometric configurations and structural parameters are shown in Fig. 1.

For bare $Ni^+$, it has a doublet ground state with the $^2D(d^9) \rightarrow {}^4F(d^8s^1)$ excitation energy of 20.1 (calcd) and 24.9 (expt) kcal/mol [57]. However, $NiBr^+$ bears a high-spin ground state (triplet). NBO analysis suggests that $Ni^+$ and Br form strong polarized covalent bonds through the $4s3d(Ni^+)$ and $4s4p(Br)$ orbits. The bond in triplet comprises one $\sigma(Ni^+Br)$ and one $\beta$–$\pi(Ni^+Br)$ binding orbitals, whereas the singlet state only forms one $\sigma(Ni^+Br)$ binding orbital, which leads to a short Ni–$Br^+$ equilibrium distance [2.156 (triplet) vs 2.188 (singlet) Å] and strong diabatic BDE (74.2 vs 14.8 kcal/mol) of the triplet species and a large triplet → singlet excitation energy of 39.1 kcal/mol.

Three encounter complexes (**1a**, **1b**, and **1c**) are formed in the reaction of $NiBr^+/C_3H_8$. **1a** is featured by a $BrNi^+(\eta^4$–$C_3H_8)$ structure, where $Ni^+$ is simultaneously coordinated to 2α,2γ-H (noted as $BrNi^+(\eta^4$–2α,2γ-H–$C_3H_8)$). Both **$^1$1b** and **$^1$1c** possess a $BrNi^+(\eta^2$–α,β-H–$C_3H_8)$ structure, in which the $BrNi^+$ axis inclines to $H^\alpha$ and $H^\beta$, respectively, while **$^3$1b** and **$^3$1c** bear a respective $BrNi^+(\eta^3$–α,2β-H–$C_3H_8)$ and $BrNi^+(\eta^3$–2α,β-H–$C_3H_8)$ structure. Energetically, the diabatic BDEs of **1a**, **1b**, and **1c** are calculated to be in the range of 57.2–59.4 kcal/mol (singlet) and 43.5–41.3 kcal/mol (triplet), indicating the nearly identical stability as well as the coexistence for these isomers in the gas phase.

NBO analysis shows that the association of $NiBr^+$ with $C_3H_8$ (**1a**, **1b** and **1c**) is dominated by the electrostatic interaction as well as donor–acceptor stabilization, i.e., electrons donation from the coordinated σ(CH) orbitals to unoccupied $4s3d(Ni^+)$ and $\sigma^*(Ni^+Br)$ orbits as well as the back-donation from the filled $4s3d(Ni^+)$ orbit to the $\sigma^*$(CH) orbit [$\Delta E^{(2)}$ = 148.6 (90.2) (**1a**), 147.4 (77.7) (**1b**), and 143.7 (73.1) (**1c**) kcal/mol in the singlet (triplet)]. This results in the weakening interaction of the corresponding C–H bond and in preparation for the next step of hydrogen transfer. Furthermore, the much stronger donor–acceptor interaction in the singlet explains its stronger diabatic BDE.

$Ni(C_3H_7)^+$ is the product of HBr elimination in the reaction of $NiBr^+/C_3H_8$. It contains three kinds of isomers, i.e., **Ia** and **Ib** via α-H abstraction and **Ic** via β-H abstraction, respectively. **Ia** is featured by *cis*-$Ni^+(\eta^2$–α-C,γ-H–$CH_2CH_2CH_3)$, forming a five-membered structure, while **Ib** bears a *trans*-$Ni^+(\eta^1$–α-C–$CH_2CH_2CH_3)$ structure. For **Ic**, the metal ion strongly binds to the radical $C^\beta$ atom of $CH_3CHCH_3$ (noted as $Ni^+(\eta^1$–β-C–$CH_2CH_2CH_3)$). Although the nearest $Ni^+$–C distances in **$^3$Ia** − **$^3$Ic** (1.93–1.97 Å) are calculated to be longer than those in the singlet (1.86–1.87 Å), the triplet diabatic BDEs are larger than those of the singlet [84.0 vs 61.4 (**Ia**), 81.0 vs 63.3 (**Ib**), 80.5 vs 64.5 (**Ic**) kcal/mol]. This is because that the diffuse single-occupied 4*s* orbital in $Ni^+(^4F(d^8s^1))$ favors forming a relative strong covalent bond with the *radical*-C atom of $C_3H_7$. NBO analysis shows that the $Ni^+$–$(C_3H_7)$ association is dominated by the covalent interaction via a $\sigma(Ni^+C)$ binding orbital, which is consisted by the $2p$(*radical*-C) orbital and the $3d(Ni^+)$ orbital in the singlet and the α-4*s* and β-$3d(Ni^+)$ orbitals in the triplet.

For the $H_2$-loss product, two candidates can be envisaged: $BrNi(CH_2CH_2CH_2)^+$ complex (**Ja**) via α,γ-H abstraction and $BrNi(CH_2CHCH_3)^+$ complex (**Jb**) via α,β- and β,α-H abstractions. In **$^1$Ja**, $Ni^+$ of $NiBr^+$

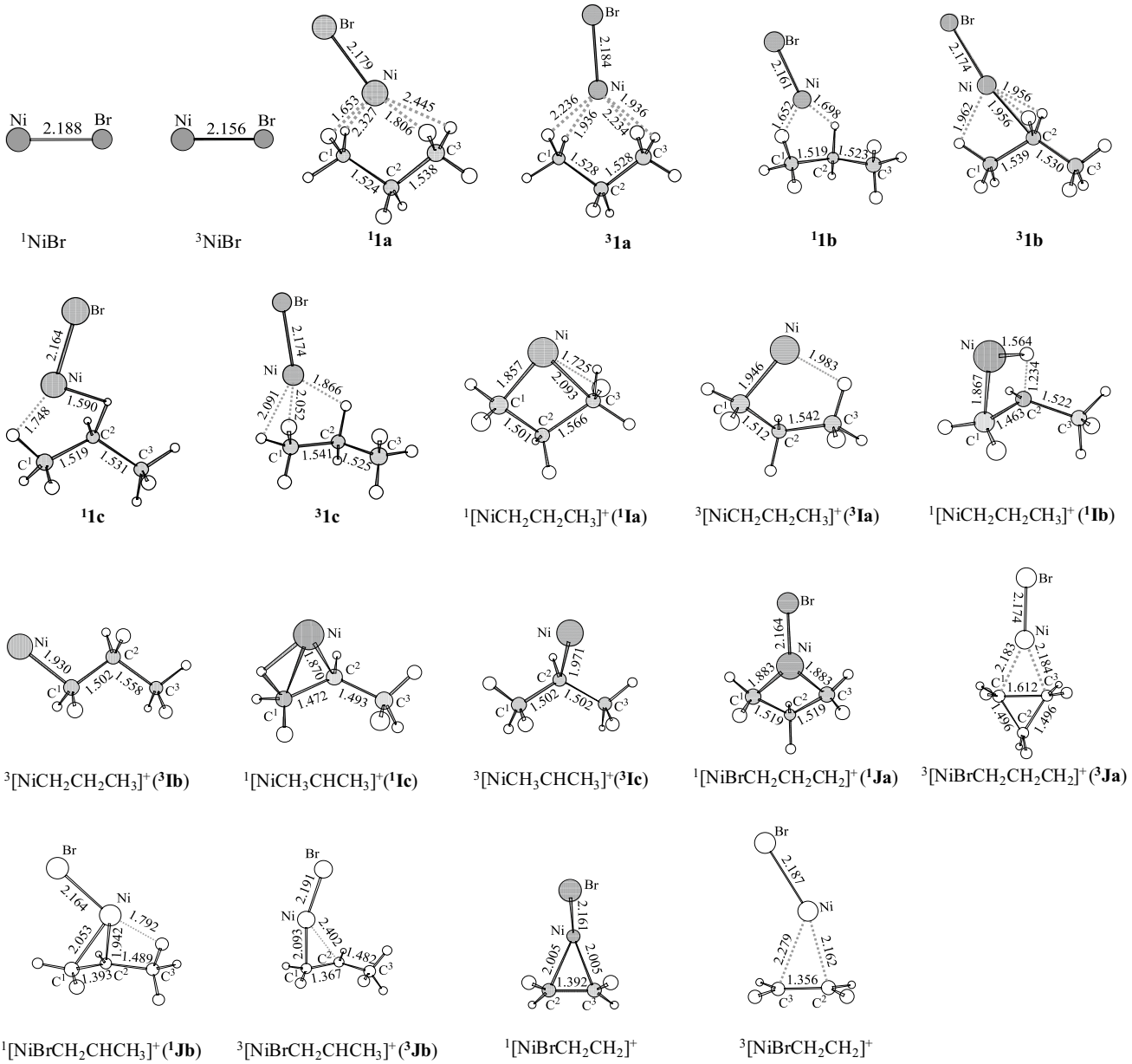


**Fig. 1** Geometries and selected structural parameters optimized at the B3LYP: B3LYP/DZVP(*d*)(opt + 3*f*): 6-311++G(2*d*,2*p*) level for the reactants, encounter complexes, and some product species involved in the $NiBr^+$ + propane reaction. Bond lengths are in angstroms, and bond angles are in degrees

simultaneously attacks at both terminal C atoms of $CH_2CH_2CH_2$ (with $Ni^+$–C distance of 1.883 Å), forming a *quadrilateral*-type structure. In the triplet, however, the $C_3H_6$ ligand forms a cyclopropane structure and $NiBr^+$ is coordinated to one side of cyclopropane. The corresponding diabatic BDE is calculated to be 74.0 and 51.2 kcal/mol in its singlet and triplet states, respectively. NBO analysis suggests that the metal ion in the singlet state forms two strong polarized covalent bonds with two-coordinated C atoms, while the association of $NiBr^+$ with $C_3H_6$ in the triplet state is dominated by electrostatic interaction as well as donor–acceptor stabilization ($\Delta E^{(2)}$ = 65.3 kcal/mol). The triplet $BrNi^+(CH_2CHCH_3)$ (**Jb**) is featured by an alkenyl-CC $\pi$-type bound structure (with $Ni^+$–C distances of 2.093 and 2.402 Å) ($\Delta E^{(2)}$ = 70.4 kcal/mol), while the singlet counterpart favors a multicenter association of metal ion with $C^{\alpha}$, $C^{\beta}$, and $H^{\gamma}$ of $C_3H_6$ (with distances of 2.053, 1.942, and 1.792 Å, respectively), suggesting the stronger interactions of metal with both the alkenyl-$\pi$ and $\sigma(C^{\gamma}H)$ orbitals ($\Delta E^{(2)}$ = 115.6 and 41.9 kcal/mol, respectively). Thus, the diabatic BDE of the singlet (81.7 kcal/mol) is stronger than that of the triplet (55.4 kcal/mol).

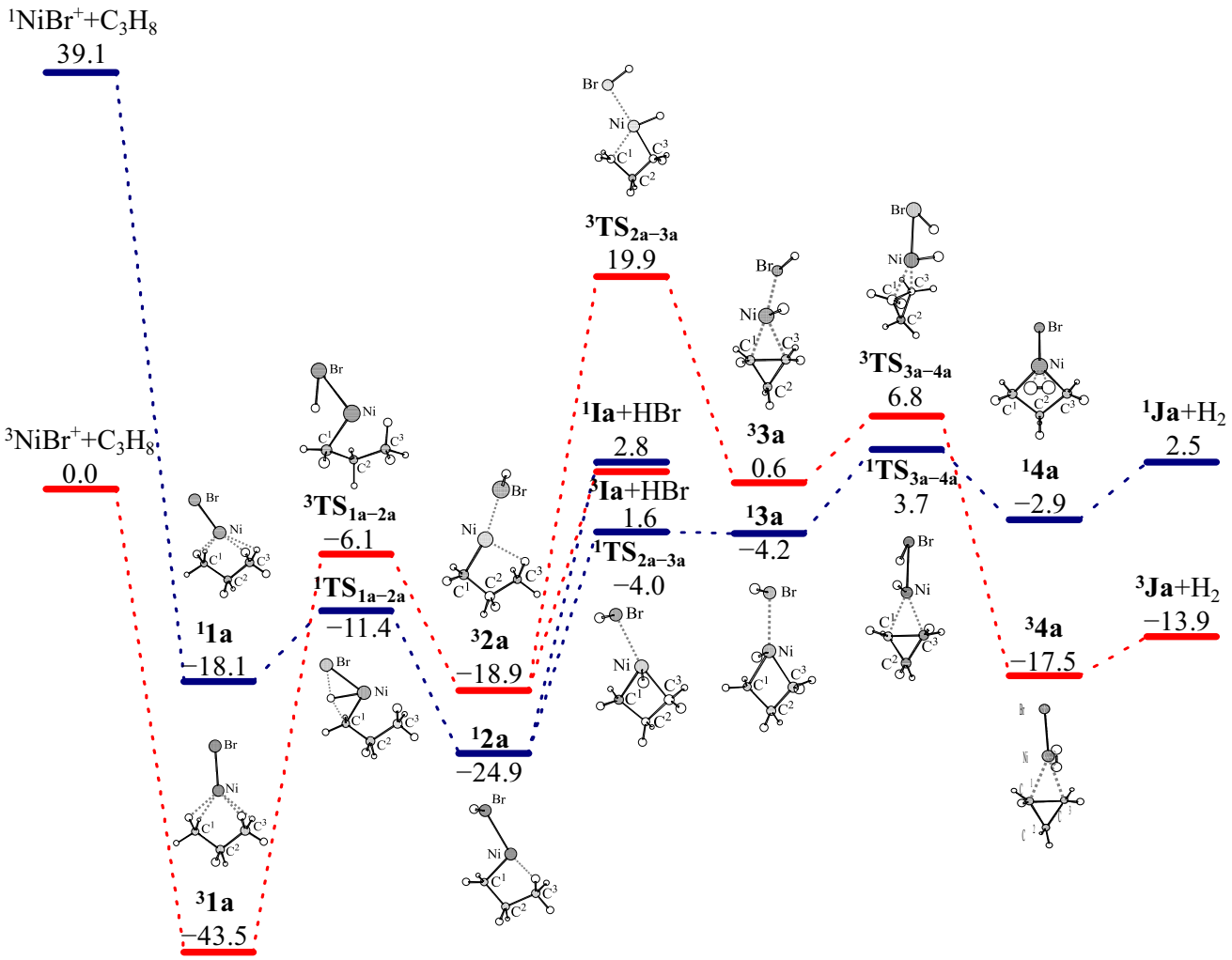


**Fig. 2** Energy profile for the $\alpha,\gamma$-H abstraction mechanism involved in the reaction of $NiBr^+$ with propane. *Numbers* refer to the relative stabilities with respect to the separated reactants of $^3NiBr^+$ + propane evaluated at the B3LYP/DZVP(*d*)(opt + 3*f*): 6-311++G(2*d*,2*p*) level including ZPE corrections. Scaling factor for the ZPE is 0.961. Relative energies are in kcal/mol

$BrNi(CH_2CH_2)^+$ is the C–C activation product via loss of methane. In both multiplicities, the species have the $C_s$ symmetry and $NiBr^+$ attaches the two ethylene C atoms simultaneously through the metal with the difference that the $NiBr^+$ bond in the triplet is co-plane with the $Ni^+CC$ plane, whereas the singlet association favors an out-of-plane location of the $NiBr^+$ bond (the dihedral angle of $NiBr^+$ with the $Ni^+CC$ plane is 94.9°). This association results in elongation of the C–C bond as well as distortion of the C–C–H angle (especially for the singlet species). NBO analysis indicates that the complex is stabilized by the electron donor–acceptor interaction, i.e., donation of $\pi(CC) \rightarrow 4s3d(Ni^+)$ and $\sigma^*(Ni^+Br)$ as well as back-donation of $4s3d(Ni^+) \rightarrow \pi^*(CC)$ ($\Delta E^{(2)} = 149.9$ (singlet) and 27.6 (triplet) kcal/mol). Compared to the triplet species, the larger donor–acceptor interaction in the singlet leads to a stronger diabatic BDE [69.8 (singlet) vs 48.2 (triplet)] as well as a larger change of structure.

## 2.3 Gas-phase reaction mechanism

In this section, we will discuss all possible mechanisms for the $H_2$, HBr, and $CH_4$ eliminations in the gas-phase reaction of $NiBr^+$ with $C_3H_8$.

### *2.3.1 Initial C–H activation*

Three possible initial C–H activation pathways for losses of $H_2$ and HBr have been surveyed, that is, $\alpha,\beta$-H, $\alpha,\gamma$-H, and $\beta,\alpha$-H abstractions. PESs together with the schematic structures involved in the reaction pathways are shown in Figs. 2, 3 and 4.

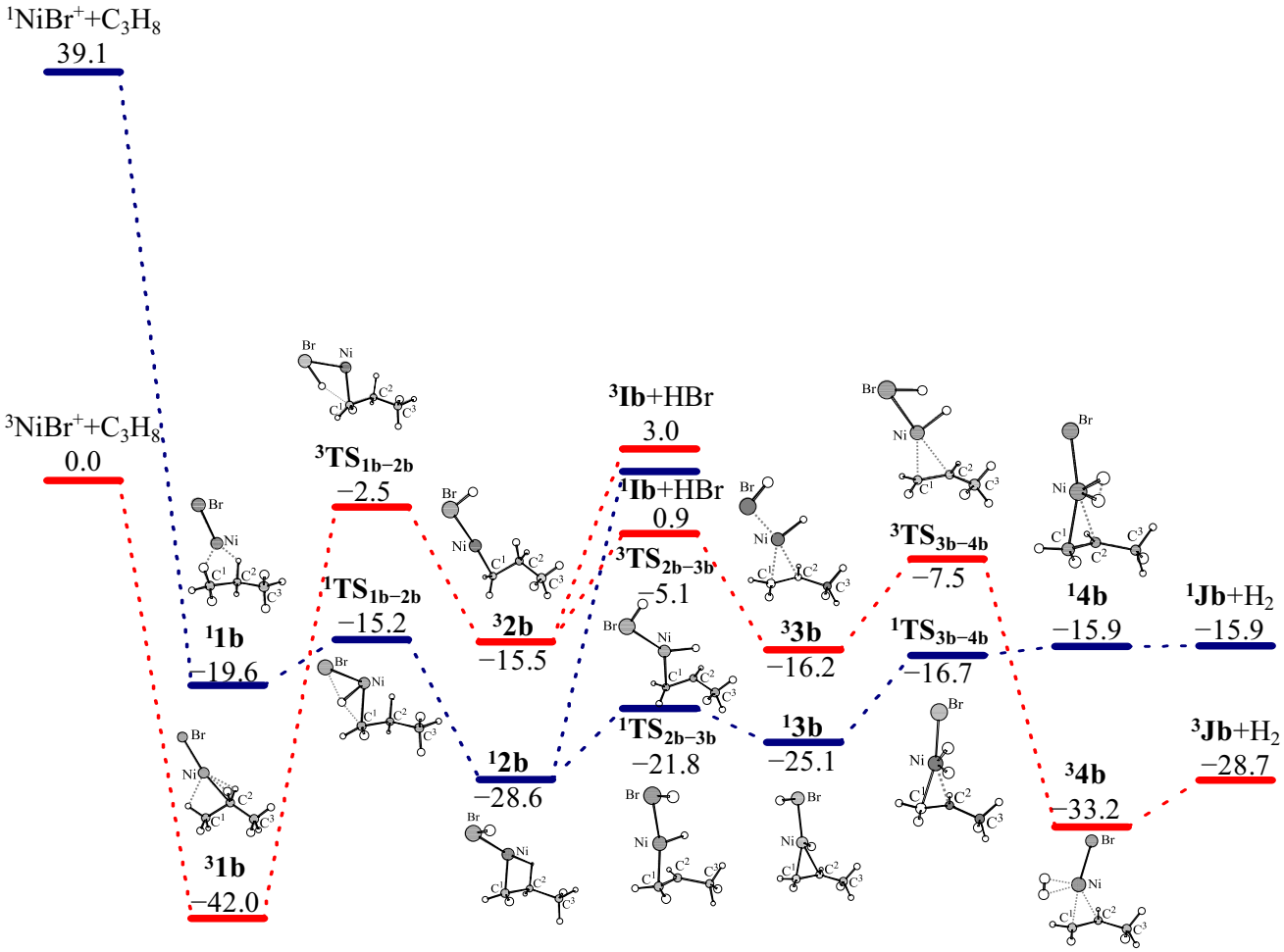


**Fig. 3** Energy profile for the $\alpha,\beta$-H abstraction mechanism involved in the reaction of $NiBr^+$ with propane. Parameters follow the same notations as in Fig. 2

*$\alpha,\gamma$-H abstraction* As shown in Fig. 2, $\alpha,\gamma$-H abstraction starts from encounter complex **1a**. **1a** could involve into species **2a** ((HBr)Ni($CH_2CH_2CH_3$)$^+$) via a $\sigma$-complex-assisted metathesis ($\sigma$-CAM) mechanism [74], which experiences a direct H-transfer from the metal-coordinated propane to the Br ligand via a four-center transition state ($\mathbf{TS_{1a-2a}}$). In this process, approaching of the metal side of $NiBr^+$ to $C_3H_8$ induces a preferential attack of $C^\alpha$–H bond and promotes the cleavage of the $C^\alpha$–H bond, subsequently through direct $C^\alpha$– to –Br hydrogen transfer **2a** is formed. The H–Br–Ni–$C^\alpha$ four-centered structure of $\mathbf{TS_{1a-2a}}$ favors forming the $\sigma(Ni^+C^\alpha)$ and $\sigma$(HBr) [$\sigma(Ni^+C^\alpha)$, $\sigma$(HBr), and $\beta$-$\sigma(Ni^+Br)$] binding orbitals in the singlet (triplet) state. Furthermore, the system is stabilized by strong electron donation of 4*p*(Br) and $\sigma$(HBr) → 4*s**($Ni^+$) and $\sigma^*(Ni^+C^\alpha)$ and back-donation of 3*d*($Ni^+$) and $\sigma(Ni^+C^\alpha)$ → $\sigma$*(HBr) ($\Delta E^{(2)}$ = 279.1 (singlet) and 69.3 (triplet) kcal/mol). It can be found that $Ni^+$ in $\mathbf{TS_{1a-2a}}$ forms one (singlet) and two (triplet) covalent bonds with the ligand and avoids binding with multi (three)-$\sigma$-type covalent ligands (for example, (Br)$Ni^+$(H)($C_2H_5$)). Thus, it is an energetically favorable process ($E_{rel}(\mathbf{TS_{1a-2a}})$ = −11.4 (singlet) and −6.1(triplet) kcal/mol).

Species **2a** is featured by a two-coordinated structure ((HBr)$Ni^+$($\eta^2$–$\alpha$-C,$\gamma$-H–$CH_2CH_2CH_3$)). Different with the binding situation in $NiBr^+$ and $BrNi^+(C_3H_8)$ (**1a**–**1c**), the metal center in **2a** involves two $\sigma$-type bonding, for which perfects pairing of electrons in preferred in the low-spin (singlet) ground state. Further NBO analysis shows that $Ni^+$ in the singlet forms strong covalent bonds with both $C_3H_7$ and HBr groups via the $\sigma(Ni^+C^\alpha)$ and $\sigma(Ni^+Br)$ binding orbitals, respectively, whereas in the triplet, the metal center only forms the covalent bond with $C_3H_7$ (via $\sigma(Ni^+C^\alpha)$) and the binding of $Ni^+$–(HBr) is dominated by donor–acceptor stabilization ($\Delta E^{(2)}$ = 72.0 kcal/mol). Thus, $^1$**2a** is 6 kcal/mol more stable than $^3$**2a** and 24.9 kcal/mol below the reactants $^3NiBr^+ + C_3H_8$.

It can be found from Fig. 2 that a triplet-to-singlet crossing occurs in the $^3$**1a** → $^1\mathbf{TS_{1a-2a}}$ process. For the

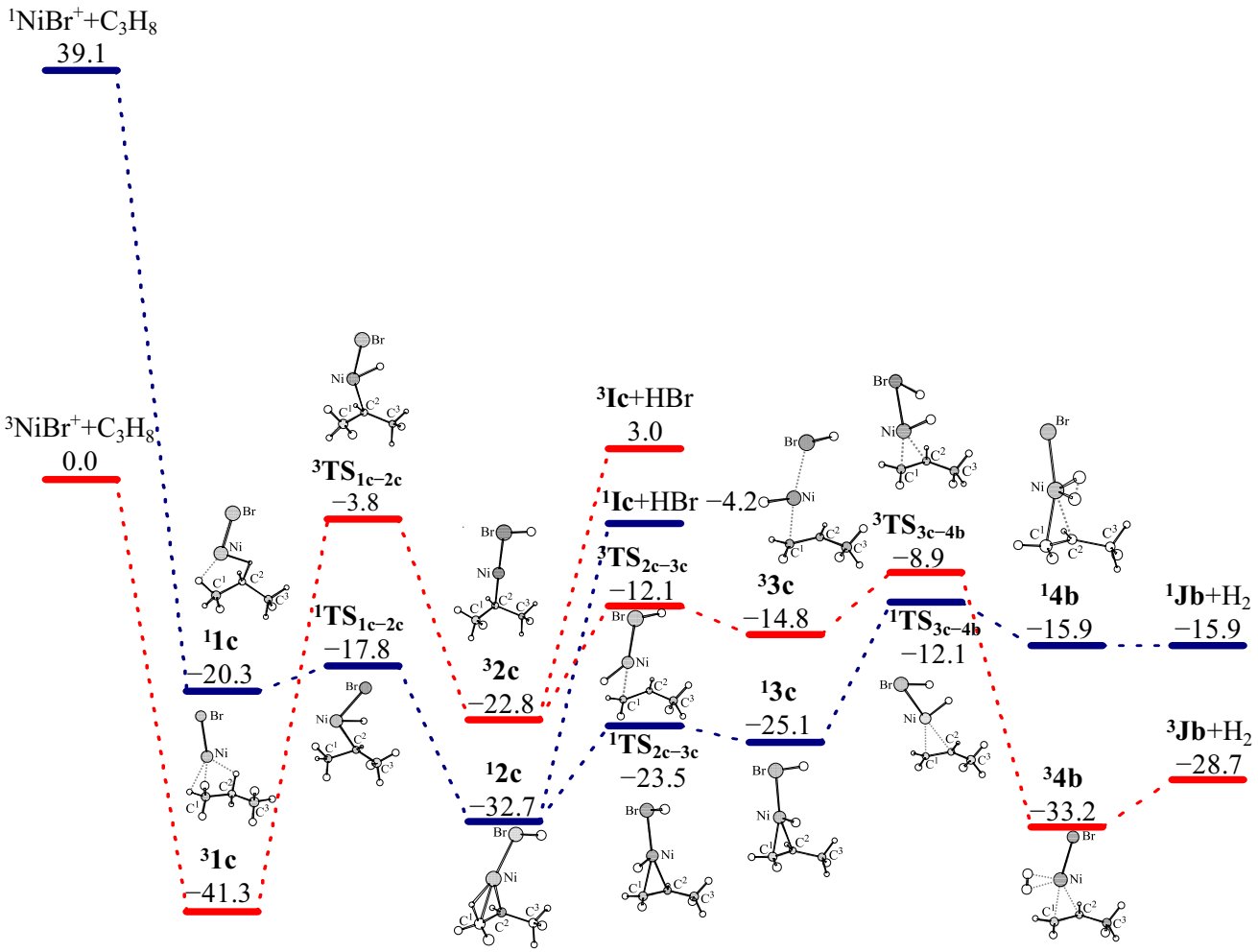


**Fig. 4** Energy profile for the $\beta,\alpha$-H abstraction mechanism involved in the reaction of $NiBr^+$ with propane. Parameters follow the same notations as in Fig. 2

relevant $MECP_{\mathbf{1a-2a}}$, the activated C–H bond is stretched to 1.184 Å, and the newly formed H–Br bond length is reduced to 2.237 Å (see Fig. S1). The SOC constant (SOCC) of $MECP_{\mathbf{1a-2a}}$ is calculated to be 133.8 $cm^{-1}$, and the crossing probability is estimated to be 59 % at the room temperature.

One exit of **2a** is the direct dissociation into $Ni(CH_2CH_2CH_3)^+$ (**Ia**) and HBr, with the whole endothermicity of 2.8 (2.5) kcal/mol on the singlet (triplet) PES. The other is yielding **3a** via a $H^\gamma$ transfer to metal center. The corresponding transition state $\mathbf{TS_{2a-3a}}$ is located at −4.0 (19.9) kcal/mol on the singlet (triplet) PES. Species **3a** bears a $(HBr)Ni^+(H)(\eta^2\text{–}\alpha,\gamma\text{-C–}CH_2CH_2CH_2)$ structure, which is located at −4.2 (singlet) and 0.6 (triplet) kcal/mol. NBO analysis shows that $Ni^+$ in $^1$**3a** forms strong covalent bonds with all three coordinated ligands via the $\sigma(Ni^+Br)$, $\sigma(Ni^+H)$, $\sigma(Ni^+C^\alpha)$, and $\sigma(Ni^+C^\gamma)$ binding orbitals, whereas in $^3$**3a,** metal center only binds covalently with the H and HBr groups via the $\sigma(Ni^+H)$ and $\beta\text{–}\sigma(Ni^+Br)$ binding orbitals, respectively, and the association of $Ni^+\text{–}(C_3H_6)$ is stabilized by donor–acceptor interaction ($\Delta E^{(2)} = 46.3$ kcal/mol).

Along reaction coordination, **3a** could involve into complex **4a** ($(Br)Ni^+(H_2)(\eta^2\text{–}\alpha,\gamma\text{-C–}CH_2CH_2CH_2)$) via a direct hydrogen coupling between the HBr and $Ni^+H$ groups. The transition state $\mathbf{TS_{3a-4a}}$ in this process lies at 3.7 (6.8) kcal/mol in the singlet (triplet) state. Both two spin structures of **4a** have $C_s$ symmetry, and two H atoms that absorbed on $Ni^+$ have formed covalent bond. The difference is that the H–H bond is co-plane with the $Br\text{–}Ni^+\text{–}C^\beta$ symmetry plane in the singlet and perpendicular in the triplet. Different with a low-spin ground state of **3a**, $^3$**4a** ($E_{rel} = -17.5$ kcal/mol) is 14.6 kcal/mol more stable than $^3$**2a**. Subsequently, **4a** could form $BrNi(CH_2CH_2CH_2)^+$ (**Ja**) and $H_2$ via a direct dissociation. The overall reaction is endothermic by 2.5 kcal/mol on the singlet PES and exothermic by 13.9 kcal/mol on the triplet PES.

*α,β-H abstraction* α,β-H abstraction begins with **1b** (see Fig. 3). $NiBr^+$ attacks $C^{\alpha}$–H bond of $C_3H_8$ in **1b** induces H shift from $C^{\alpha}$ to Br, yielding **2b**. **2b** is also featured by a two-coordinated structure [$(HBr)Ni^+(\eta^1$–α-C–$CH_2CH_2CH_3)$], which favors a low-spin (singlet) ground state ($E_{rel}$ = −28.6 (singlet) and −15.5 (triplet) kcal/mol). The corresponding transition state $\mathbf{TS_{1b-2b}}$ is located at −15.2 and −2.5 kcal/mol on the singlet and triplet PESs, respectively. Thus, a triplet-to-singlet crossing is expected to occur immediately before $\mathbf{TS_{1b-2b}}$. The relevant $\mathbf{MECP_{1b-2b}}$ is located when the activated C–H bond is stretched to 1.204 Å, and the newly formed H–Br bond length is reduced to 2.181 Å. The SOCC of $\mathbf{MECP_{1b-2b}}$ is calculated to be 127.6 $cm^{-1}$, and the crossing probability is found to be 64 %.

Direct decomposition of (HBr)–$Ni^+(CH_2CH_2CH_3)$ accounts for $Ni(CH_2CH_2CH_3)^+$ (**Ib**) + HBr, but it is a slight endothermic channel with a reaction heat of 0.9 (3.0) kcal/mol on the singlet (triplet) PES. Alternatively, direct $C^{\beta}$-to-$Ni^+$ H-shift from **2b** could yield species **3b** ((HBr)$Ni^+(H)(\eta^2$–α,β-C–$CH_2CHCH_3$)). In both multiplicities, the 3*d*($Ni^+$) and 1*s*(H) orbitals form a σ($Ni^+$H) binding orbital, while the linkage of metal center with the other two groups (HBr and $CH_2CHCH_3$) is strengthened by the strong electron donation from the 4*s*4*p*(Br) and π(CC) orbitals to 4*s*4*p*($Ni^+$) orbitals as well as back-donation from the 3*d*($Ni^+$) orbital to the π*(CC) orbital ($\Delta E^{(2)}$ = 256.7 (singlet) and 150.8 (triplet) kcal/mol). Energetically, species **3b** is located at −25.1 (−16.2) kcal/mol on the singlet (triplet) PES, while the relevant transition state ($\mathbf{TS_{2-3b}}$) lies at −21.8 (−5.1) kcal/mol.

Subsequently, species **3b** involves into molecular hydrogen complex **4b** ((Br)$Ni^+(H_2)(\eta^2$–α,β-C–$CH_2CHCH_3$)). Mainly, electrostatic interaction as well as donor–acceptor stabilizations for the ($H_2$)–$BrNi^+$–($CH_2CHCH_3$) association results in a triplet ground state for **4b**, similar to $NiBr^+$ (excitation energy for $^3$**4b** → $^1$**4b**: 17.3 kcal/mol). The situation of transition state $\mathbf{TS_{3b-4b}}$ is a compromise between **3b** and **4b**, where the triplet transition state lies above the singlet one by 9.2 kcal/mol. Loss of $H_2$ from **4b** accounts for $BrNi^+(CH_2CHCH_3)$ (**Jb**), exothermic by 15.9 (28.7) kcal/mol in the singlet (triplet) state.

*β,α-H abstraction* β,α-H abstraction pathway starts with **1c** (see Fig. 4). Direct $C^{\beta}$– to –Br hydrogen shift could carry **1c** into **2c** ((HBr)$Ni^+(\eta^1$–β-C–$CH_3CHCH_3$)), which also favors a singlet ground state [$E_{rel}$ = −32.7 (singlet) and −22.8 (triplet)]. The relevant transition state $\mathbf{TS_{1c-2c}}$ is located at −17.8 (−3.8) kcal/mol on the singlet (triplet) PES. As shown in Fig. 4, a triplet-to-singlet crossing occurs in the $^3$**1c** → $^1\mathbf{TS_{1c-2c}}$ process. The activated C–H bond and newly formed H–Br bond in the relevant $\mathbf{MECP_{1c-2c}}$ are calculated to be 1.221 and 2.243 Å, respectively (see Fig. S1). The SOCC of $\mathbf{MECP_{1c-2c}}$ is calculated to be 134.3 $cm^{-1}$, and the crossing probability is estimated to be 73 % at the room temperature, indicating that the β,α-H abstraction accounts for the most large crossing probability in all three H abstraction mechanisms.

Direct loss of HBr from **2c** accounts for $Ni(CH_3CHCH_3)^+$ (**Ic**), which is exothermic by 4.2 kcal/mol on the singlet PES and endothermic by 3.0 kcal/mol on the triplet PES. The other exit of **2c** is α-H shift to metal center forming **3c**. Similar to **3b**, **3c** is featured by a (HBr)$Ni^+(H)(\eta^2$–α,β-C–$CH_2CHCH_3$) structure and bears singlet as ground state ($E_{rel}$ = −25.1 (singlet) and −14.8 (triplet) kcal/mol). The relevant transition state $\mathbf{TS_{2c-3c}}$ is located at −23.5 (−12.1) kcal/mol on the singlet (triplet) PES. Subsequently, direct H coupling between the BrH and $Ni^+$H groups carries **3c** into **4b** via transition state $\mathbf{TS_{3c-4c}}$ (lying at −12.1 (singlet) and −8.9 (triplet) kcal/mol). Direct loss of $H_2$ from **4b** forming $BrNi(CH_2CHCH_3)^+$ (**Jb**) has been discussed above.

From Figs. 2, 3, 4 and 5, we can find that all of the α,β-, α,γ-, and β,α-H abstraction mechanisms could account for losses of HBr and $H_2$. Two spin crossing occurs in all three mechanisms, that is, initial C–H activation and hydrogen coupling. The probability of the former crossing is calculated to be 64, 59, and 73 % for the α,β-, α,γ-, and β,α-H abstraction mechanisms, respectively, indicating that the triplet pathway can easily proceed to the singlet surface near the intersection, which reduced the reaction energy barrier. In all three H abstraction mechanisms, the most favorable mechanism is the β,α-H abstraction because it is not only energetically favorable but could also take place adiabatically on both the singlet and triplet PESs. If the underestimate of the stability of the HBr + $[C_3, H_7, Ni]^+$ exit channel (about 13 kcal/mol) is considered, loss of HBr is also a strong exothermic process for all three H abstraction mechanisms. Furthermore, the HBr-loss pathway is much simple compared to that of loss of $H_2$. Therefore, the $HBr/H_2$ branching ratio of 58:42 is determined by the ESI mass spectrum experiment [38].

### 2.4 Initial C–C activation

We also considered the C–C activation pathway to loss of $CH_4$. PES together with schematic structures involved in the reaction is shown in Fig. 5. This channel involves encounter complex **1b**. Starting with **1b**, the nickel ion inserts into one C–C bond of propane forming species **2d** ($(CH_3)Ni^+(Br)(CH_2CH_3)$) via transition state $\mathbf{TS_{1b-2d}}$. In this process, metal center involves three σ-type bonding (with Br, $CH_3$, and $CH_2CH_3$), which is unfavorable for $Ni^+$($^2$D($d^9$) and $^4$F($d^8s^1$). NBO analysis indicates that $Ni^+$ in both $^1\mathbf{TS_{1b-2d}}$ ($^3\mathbf{TS_{1b-2d}}$) and $^1$**2d** ($^3$**2d**) has a high population of 4*p* orbital ($3d^{8.72}4s^{0.29}4p^{0.53}$ ($3d^{8.46}4s^{0.48}4p^{0.25}$) and $3d^{8.72}4s^{0.35}4p^{0.39}$ ($3d^{8.59}4s^{0.36}4p^{0.43}$)). Therefore,

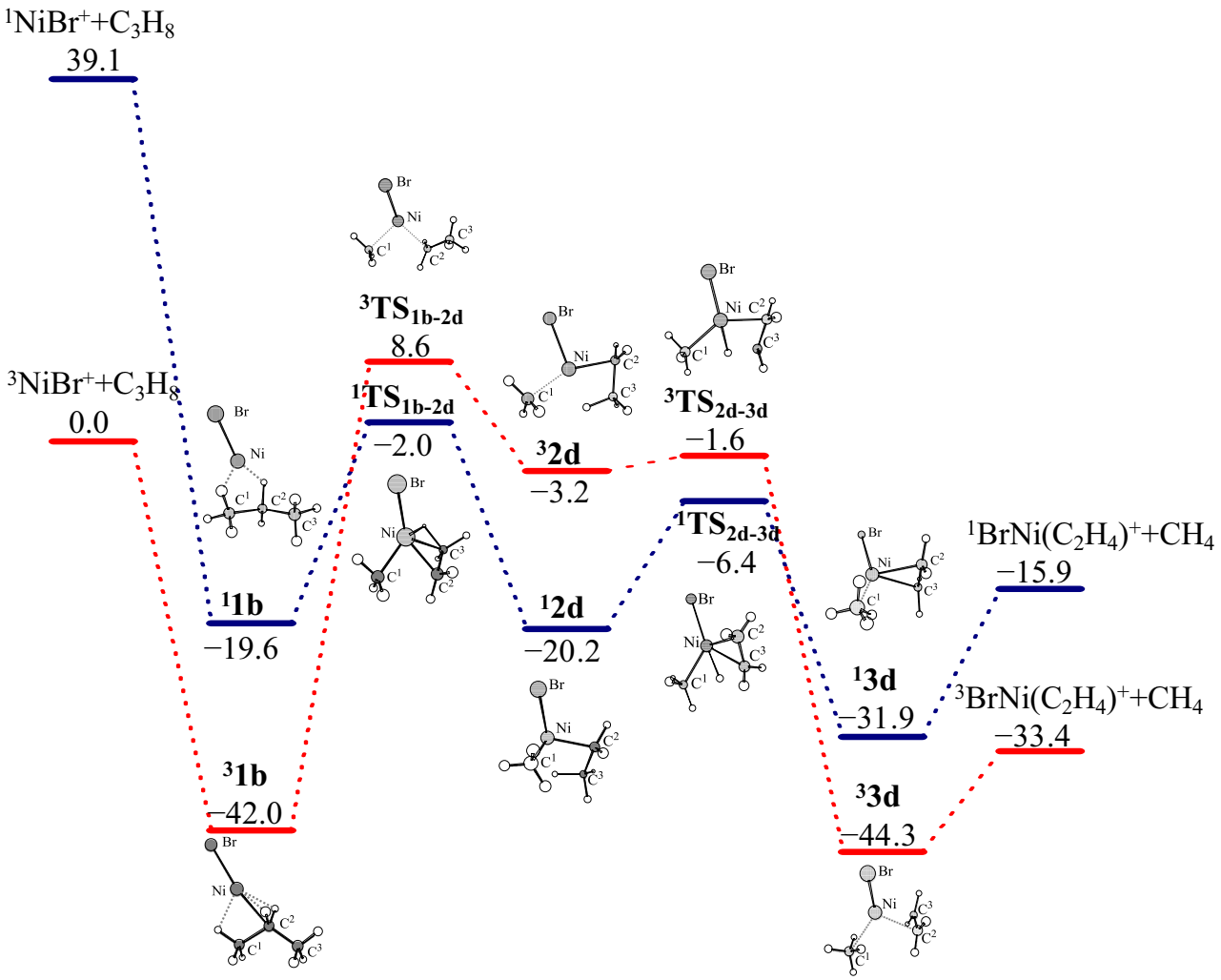


**Fig. 5** Energy profile for the initial C–C activation involved in the reaction of $NiBr^+$ with propane. Parameters follow the same notations as in Fig. 2

it is a high-energy pathway [$E_{rel}$(**TS$_{1b-2d}$** and **2d**) = −2.0 (+8.6) and −20.2 (−3.2) kcal/mol in the singlet (triplet)]. PES shows that a triplet-to-singlet crossing emerges before **TS$_{1b-2d}$**. The relevant SOCC is calculated to be 116.7 $cm^{-1}$ with the crossing probability of 45 %.

A subsequent $\beta$-H shift to methyl could form species **3d** via transition state **TS$_{2b-3d}$** ($E_{rel}$ = −6.4 (singlet) and −1.6 (triplet) kcal/mol). Species **3d** bears a $(CH_4)Ni^+(Br)(\eta^2\text{–}C,C\text{–}CH_2CH_2)$ structure, lying at −44.3 and −31.9 kcal/mol on the singlet and triplet PES, respectively. **3d** undergoes direct bond cleavage forming $CH_4$ and $BrNi(C_2H_4)^+$, with the whole exothermicity of 15.9 (33.4) kcal/mol on the singlet (triplet) PES.

As shown in Fig. 5, we can found that although loss of $CH_4$ is an exothermic process, it needs to overcome a high-energy barrier in the initial C–C activation [$E_{rel}$(**TS$_{1b-2d}$**) = −2.0 (+8.6) kcal/mol in the singlet (triplet)], which is 15.8 (12.4) kcal/mol higher than that of the initial $C^\beta$-H abstraction (**TS$_{1c-2c}$**). As it is well known from the Arrhenius formula for the evaluation of kinetics, a difference of about 10 kcal/mol between two barriers implies that rates change by several orders of magnitude. Thus, it is quite clear that why HBr and $H_2$ are formed in the $BrNi^+/C_3H_8$ reaction and $CH_4$ not.

It is well known that $Ni^+$ has a ground and excited electron configuration of $^2D(d^9)$ and $^4F(d^8s^1)$, respectively, suggesting that it is unfavorable forming multi-$\sigma$-type bonding with other covalent ligands. When introducing an open-shell Br ligand to $Ni^+$, the initial C–C activation of propane by $BrNi^+$ needs to experience an unfavorable three $\sigma$-type bonding (with Br, $CH_3$, and $CH_2CH_3$), resulting in the reaction being restrained. However, the initial C–H activation favors a $\sigma$-CAM mechanism, where the ligand of Br could direct abstract a H from the propane substrate through a four-center transition state, without forming multi-$\sigma$-type bonds of metal center, explaining the favorable C–H

activation for the HBr and $H_2$ losses in the reaction of $BrNi^+/C_3H_8$.

## 3 Conclusions

DFT has investigated the reaction of $NiBr^+/C_3H_8$, which add new insight into the experimental observations. We can make a conclusion by summarizing some of the main points in the following: Both HBr and $H_2$ could be formed via three initial C–H activation mechanisms, that is, $\alpha,\beta$-, $\alpha,\gamma$-, and $\beta,\alpha$-H abstractions, where the most favorable mechanism is the $\beta,\alpha$-H abstraction. Losses of HBr and $H_2$ are favored by undergoing a four-center transition state in the initial C–H activation process, avoiding forming multi-$\sigma$-type bonding of metal center. However, loss of $CH_4$ is prevented by experience unfavorable three $\sigma$-type bonding of $Ni^+$ (with Br, $CH_3$, and $CH_2CH_3$) in the initial C–C activation process.

## 4 Supporting information

Detailed description of spin–orbit coupling calculations, geometries and selected structural parameters of MECPs, and optimized geometries, selected structural parameters, calculated energies, zero-point energies, and $\langle S^2 \rangle$ for all species involved in the reaction of $NiBr^+$ with propane.

**Acknowledgments** This work was supported by the Program for NSFC (21003158 and 21303266), Shandong Province Natural Science Foundation (ZR2011EMZ002), Taishan Scholar Foundation (ts20130929), Promotive Research Fund for Excellent Young and Middle-aged Scientists of Shandong Province (BS2012NJ015), and the Fundamental Research Funds for the Central Universities (12CX02014A, 14CX02004A, and 14CX06001A).

## References

1. Russo N, Sicilia E (2001) Reaction of $Sc^+(^1D, ^3D)$ with $H_2O$, $NH_3$, and $CH_4$: a density functional study. J Am Chem Soc 123(11):2588–2596
2. Chen Q, Chen HP, Kais S, Freiser B (1997) Gas-phase reactions of $Fe(CH_2O)^+$ and $Fe(CH_2S)^+$ with small alkanes: an experimental and theoretical study. J Am Chem Soc 119(52):12879–12888
3. Sicilia E, Russo N (2002) Theoretical study of ammonia and methane activation by first-row transition metal cations $M^+$ (M = Ti, V, Cr). J Am Chem Soc 124(7):1471–1480
4. Michelini MC, Russo N, Sicilia E (2007) Gas-phase chemistry of actinides ions: new insights into the reaction of $UO^+$ and $UO_2^+$ with water. J Am Chem Soc 129(14):4229–4239
5. Irigoras A, Elizalde O, Silanes I, Fowler JE, Ugalde JM (2000) Reactivity of $Co^+(^3F,^5F)$, $Ni^+(^2D,^4F)$, and $Cu^+(^1S,^3D)$: reaction of $Co^+$, $Ni^+$, and $Cu^+$ with water. J Am Chem Soc 122(1):114–122
6. Irigoras A, Fowler JE, Ugalde JM (1999) Reactivity of $Cr^+(^6S,^4D)$, $Mn^+(^7S,^5S)$, and $Fe^+(^6D,^4F)$: reaction of $Cr^+$, $Mn^+$, and $Fe^+$ with water. J Am Chem Soc 121(37):8549–8558
7. Chiodo S, Rivalta I, Michelini MC, Russo N, Sicilia E, Ugalde JM (2006) Activation of methane by the iron dimer cation. A theoretical study. J Phys Chem A 110(45):12501–12511
8. Sunderlin LS, Armentrout PB (1988) Methane activation by $Ti^+$: electronic and translational energy dependence. J Phys Chem 92(5):1209–1219
9. MacMahon TJ, Jackson TC, Freiser BS (1989) A gas-phase study of $FeSn^+$ (n = 1–6). J Am Chem Soc 111(2):421–427
10. Sodupe M, Charles WBJ (1991) Theoretical study of the bonding of the first- and second-row transition-metal positive ions to acetylene. J Phys Chem 95(22):8640–8645
11. Blomberg MRA, Siegbahn PEM, Nagashima U, Wennerberg J (1991) Theoretical study of the activation of alkane carbon–hydrogen and carbon–carbon bonds by different transition metals. J Am Chem Soc 113(2):424–433
12. Perry JK, Ohanessian G, Goddard WA (1993) Molecular complexes of small alkanes with $Co^+$. J Phys Chem 97(20):5238–5245
13. Chen YM, Armentrout PB (1995) Guided ion beam studies of the reactions of $Ag^+$ with $C_2H_6$, $C_3H_8$, $HC(CH_3)^3$ and c-$C_3H_6$. J Phys Chem 99(29):11424–11431
14. Hornung G, Schrijder D, Schwarz H (1995) Diastereoselective gas-phase carbon–carbon bond activation mediated by "bare" $Co^+$ cations. J Am Chem Soc 117(31):8192–8196
15. Cornehl HH, Heinemann C, Schroder D, Schwarz H (1995) Gas-phase reactivity of lanthanide cations with hydrocarbons. Organometallics 14(2):992–999
16. Chen YM, Armentrout PB (1995) Activation of $C_2H_6$, $C_3H_8$, and c-$C_3H_6$ by gas-phase $Rh^+$ and the thermochemistry of Rh-ligand complexes. J Am Chem Soc 117(36):9291–9304
17. Holthausen MC, Koch WA (1996) Theoretical view on $Co^+$-mediated C–C and C–H bond activations in ethane. J Am Chem Soc 118(41):9932–9940
18. Noll RJ, Yi SS, Weisshaar JC (1998) Bimolecular $Ni^+(^2D_{5/2}) + C_3H_8$ reaction dynamics in real time. J Phys Chem A 102(2):386–394
19. Yi SS, Blomberg MRA, Siegbahn PEM, Weisshaar JC (1998) Statistical modeling of gas-phase organometallic reactions based on density functional theory: Ni++ $C_3H_8$. J Phys Chem A 102(2):395–411
20. Blomberg M, Yi SS, Noll RJ, Weisshaar JC (1999) Gas-phase Ni+ (2D5/2)+ n-$C_4H_{10}$ reaction dynamics in real time: experiment and statistical modeling based on density functional theory. J Phys Chem A 103(36):7254–7267
21. Fedorov DG, Gordon MS (2000) A theoretical study of the reaction paths for cobalt cation + propane. J Phys Chem A 104(11):2253–2260
22. Moc J, Fedorov DG, Gordon MS (2000) A theoretical study of the reaction of $Ti^+$ with ethane. J Chem Phys 112(23):10247–10258
23. Li FX, Zhang XG, Armentrout PB (2006) The most reactive third-row transition metal: guided ion beam and theoretical studies of the activation of methane by $Ir^+$. Int J Mass Spectrom 255–256:279–300
24. Armentrout PB (2006) Activation of $CH_4$ by gas-phase $Mo^+$, and the thermochemistry of Mo-ligand complexes. J Phys Chem A 110(27):8327–8338
25. Armentrout PB, Shin S, Liyanage R (2006) Guided-ion beam and theoretical study of the potential energy surface for activation of methane by $W^+$. J Phys Chem A 110(4):1242–1260
26. Armentrout PB (2007) Activation of $C_2H_6$ and $C_3H_8$ by gas-phase Mo+: thermochemistry of Mo-ligand complexes. Organometallics 26(23):5473–5485
27. Armentrout PB (2007) Activation of $C_2H_6$ and $C_3H_8$ by gas-phase Mo+: potential energy surfaces and reaction mechanisms. Organometallics 26(23):5486–5500

28. Parke LG, Hinton CS, Armentrout PB (2007) Experimental and theoretical studies of the activation of methane by $Ta^+$. J Phys Chem C 111(48):17773–17787
29. Shayesteh A, Lavrov VV, Koyanagi GK, Bohme DK (2009) Reactions of atomic cations with methane: gas phase room-temperature kinetics and periodicities in reactivity. J Phys Chem A 113(19):5602–5611
30. Lv LL, Wang YC, Geng ZY, Si YB, Wang Q, Liu HW (2009) Activation of $C_2H_6$ by gas-phase $Ta^+$: potential energy surfaces, spin-orbit coupling, spin-inversion probabilities, and reaction mechanisms. Organometallics 28(21):6160–6170
31. de Almeida KJ, Duarte HA (2010) Dehydrogenation of methane by gas-phase Th, $Th^+$, and $Th^{2+}$: theoretical insights into actinide chemistry. Organometallics 29(17):3735–3745
32. Mandich ML, Steigerwald ML, Reents WD (1986) The effects of chloro substitution on the electronic-structure of $ClCr^+$, $ClMn^+$, and $ClFe^+$ and their reactivity with small alkanes. J Am Chem Soc 108(20):6197–6202
33. Mazurek U, Schroder D, Schwarz H (1998) Generation and reactivity of chromium fluoride cations ($CrF_n^+$, n = 0–4) in the gas phase. Collect Czech Chem C 63(9):1498–1512
34. Roithova J, Schroder D (2007) Bimolecular reactions of molecular dications: new reactivity paradigms and bond-forming processes. Phys Chem Chem Phys 9(19):2341–2349
35. Schroder D, Hrusak J, Schwarz H (1993) Ligand effects on the reactivity of iron (II) cations $FeX^+$ in the gas phase. Ber Bunsenges Phys Chem 97(9):1085–1090
36. Mandich ML, Steigerwald ML, Reents WD (1986) The effects of chloro substitution on the electronic-structure of ClCr, ClMn, and ClFe and their reactivity with small alkanes. J Am Chem Soc 108(20):6197–6202
37. Mazurek U, Schroder D, Schwarz H (1998) Generation and reactivity of chromium fluoride cations (CrFn, n = 0–4) in the gas phase. Coll Czech Chem Comm 63:1498–1512
38. Schlangen M, Schwarz H, Schroder D (2007) Ligand and substrate effects in gas-phase reactions of $NiX^+$/RH Couples (X = F, Cl, Br, I; R = $CH_3$, $C_2H_5$, n-$C_3H_7$, n-$C_4H_9$). Chem Eur J 13(24):6810–6816
39. Becke AD (1993) Density-functional thermochemistry. III. The role of exact exchange. J Chem Phys 98(7):5648–5652
40. Lee C, Yang W, Parr RG (1988) Development of the Colle–Salvetti correlation-energy formula into a functional of the electron density. Phys Rev B 37:785–789
41. Chiodo S, Russo N, Sicilia E (2005) Newly developed basis sets for density functional calculations. J Comput Chem 26:175–183
42. Frisch MJ, Pople JA, Binkley JS (1984) Self-consistent molecular orbital methods 25. Supplementary functions for Gaussian basis sets. J Chem Phys 80:3265–3269
43. Zhao LM, Liu ZC, Guo WY, Lu XQ, Lin XQ, Shan HH (2008) Mechanisms for the $Ni^+$-mediated oxidation of benzene to phenol by $N_2O$. Chem Phys Lett 463:54–59
44. Rondinelli F, Russo N, Toscano M (2007) On the origin of the different performance of iron and manganese monocations in catalyzing the nitrous oxide reduction by carbon oxide. Inorg Chem 46:7489–7493
45. Glendening ED, Reed AE, Carpenter JE, Weinhold F NBO Version 3.1
46. Reed AE, Curtiss LA, Weinhold F (1988) Intermolecular interactions from a natural bond orbital, donor–acceptor viewpoint. Chem Rev 88(6):899–926
47. Grimme S (2011) Density functional theory with London dispersion corrections. WIREs Comput Mol Sci 1(2):211–228
48. Chai JD, Head-Gordon M (2008) Long-range corrected hybrid density functionals with damped atom–atom dispersion corrections. Phys Chem Chem Phys 10:6615–6620
49. Stefan G (2006) Semiempirical GGA-type density functional constructed with a long-range dispersion correction. J Comput Chem 27(15):1787–1799
50. Frisch MJ, Trucks GW, Schlegel HB, Scuseria GE, Robb MA, Cheeseman JR, Scalmani G, Barone V, Mennucci B, Petersson GA, Nakatsuji H, Caricato M, Li X, Hratchian HP, Izmaylov AF, Bloino J, Zheng G, Sonnenberg JL, Hada M, Ehara M, Toyota K, Fukuda R, Hasegawa J, Ishida M, Nakajima T, Honda Y, Kitao O, Nakai H, Vreven T, Montgomery JJA, Peralta JE, Ogliaro F, Bearpark MJ, Heyd J, Brothers EN, Kudin KN, Staroverov VN, Kobayashi R, Normand J, Raghavachari K, Rendell AP, Burant JC, Iyengar SS, Tomasi J, Cossi M, Rega N, Millam NJ, Klene M, Knox JE, Cross JB, Bakken V, Adamo C, Jaramillo J, Gomperts R, Stratmann RE, Yazyev O, Austin AJ, Cammi R, Pomelli C, Ochterski JW, Martin RL, Morokuma K, Zakrzewski VG, Voth GA, Salvador P, Dannenberg JJ, Dapprich S, Daniels AD, Farkas Ö, Foresman JB, Ortiz JV, Cioslowski J, Fox DJ (2009) Gaussian 09. Gaussian, Wallingford
51. Li YY, Guo WY, Zhao LM, Liu ZC, Lu XQ, Shan HH (2012) Theoretical investigation of the reaction of $Mn^+$ with ethylene oxide. J Phys Chem A 116(1):512–519
52. Schmidt MW, Baldridge KK, Boatz JA, Elbert ST, Gordon MS, Jensen JH, Koseki S, Matsunaga N, Nguyen KA, Su SJ, Windus TL, Dupuis M, Montgomery JA (1993) General atomic and molecular electronic structure system. J Comput Chem 14:1347–1363
53. Matsunaga N, Koseki S, Gordon MS (1996) Relativistic potential energy surfaces of $XH_2$(X = C, Si, Ge, Sn, and Pb) molecules: coupling of $^1A_1$ and $^3B_1$ states. J Chem Phys 104:7988–7996
54. Zener C (1932) Non-adiabatic crossing of energy levels. Proc R Soc Lond Ser A 137:696–702
55. Zener C (1933) Dissociation of excited diatomic molecules by external perturbations. Proc R Soc Lond Ser A 140:660–668
56. Fedorov DG, Koseki S, Schmidt MW, Gordon MS (2003) Spin–orbit coupling in molecules: chemistry beyond the adiabatic approximation. Int Rev Phys Chem 22:551–592
57. Moore CE (1952) Atomic energy levels, national bureau of standards. US Government Printing Office, Washington
58. Luo YR (2007) Comprehensive handbook of chemical bond energies. CRC Press, Boca Raton
59. Rodríguez-Santiago L, Sodupe M, Tortajada J (2001) Gas-phase reactivity of $Ni^+$ with glycine. J Phys Chem A 105(22):5340–5347
60. Carpenter CJ, van Koppen PAM, Bowers MT (1995) Details of potential energy surfaces involving C–C bond activation: reactions of $Fe^+$, $Co^+$, and $Ni^+$ with acetone. J Am Chem Soc 117(44):10976–10985
61. Rodríguez-Santiago L, Noguera M, Sodupe M, Salpin JY, Tortajada J (2003) Gas phase reactivity of $Ni^+$ with urea. Mass spectrometry and theoretical studies. J Phys Chem A 107(46):9865–9874
62. Rodríguez-Santiago L, Tortajada J (2002) Experimental and theoretical studies on the gas phase reactivity of formamide-$Ni^+$ complexes generated by FAB and electrosprayionization. Int J Mass Spectrom 219:429–443
63. Armentrout PB, Beauchamp JL (1980) Endothermic reactions of $Ni^+$ with $H_2$, HD and $D_2$. Chem Phys 50(1):37–43
64. Liu F, Zhang XG, Armentrout PB (2005) Activation of $CH_4$ by gas-phase $Ni^+$ and the thermochemistry of Ni-ligand complexes. Phys Chem Chem Phys 7:1054–1064
65. Zhang Q, Kemper PR, Bowers MT (2001) $Fe(CH_4)_n^+$ and $Ni(CH_4)_n^+$ clusters: experimental and theoretical bond energies for n = 1–6. Int J Mass Spectrom 210–211:265–281
66. Sievers MR, Jarvis LM, Armentrout PB (1998) Transition-metal ethene bonds: thermochemistry of M+ $(C_2H_4)_n$ (M = Ti–Cu, n = 1 and 2) complexes. J Am Chem Soc 120:1891–1899

67. Hanratty MA, Beauchamo JL, Illies AJ, Koppen PV, Bowers MT (1988) Kinetic energy release distributions as a probe of transition-metal-mediated hydrogen–hydrogen, carbon–hydrogen, and carbon–carbon bond formation processes: reactions of cobalt and nickel ions with alkanes. J Am Chem Soc 110(1):1–14
68. Fisher ER, Armentrout PB (1990) Reactions of $Co^+$, $Ni^+$, and $Cu^+$ with cyclopropane and ethylene oxide. Metal–methylidene ion bond energies. J Phys Chem 94(4):1674–1683
69. Allison J, Ridge DP (1979) Reactions of atomic metal ions with alkyl halides and alcohols in the gas phase. J Am Chem Soc 101:4998–5009
70. Zhao LM, Lu XQ, Li YY, Chen J, Guo WY (2012) On the gas-phase $Co^+$-mediated oxidation of ethane by $N_2O$: a mechanistic study. J Phys Chem A 116(12):3282–3289
71. Holthausen MC, Koch WA (1996) Theoretical view on Co-mediated C–C and C–H bond activations in ethane. J Am Chem Soc 118:9932–9940
72. Holthausen MC, Fiedler A, Schwarz H, Koch W (1996) How does $Fe^+$ activate C–C and C–H Bonds in ethane? A theoretical investigation using density functional theory. J Phys Chem 100:6236–6242
73. Zhao LM, Guo WY, Liu ZC, Li YY, Lu XQ (2011) Theoretical study of the gas-phase $Fe^+$-mediated oxidation of ethane by $N_2O$. Theor Chem Acc 128:349–358
74. Perutz RN, Sabo-Etienne S (2007) The σ-CAM mechanism: σ-complexes as the basis of σ-bond metathesis at late-transition-metal centers. Angew Chem Int Ed 46:2578–2592